Наносистеми, наноматеріали, нанотехнології
Nanosistemi, Nanomateriali, Nanotehnologii
2022, т. 20, № 2, сс. 459–472

PACS numbers: 68.37.Hk, 78.30.-j, 78.40.-q, 81.07.-b, 81.16.Hc, 82.33.Vx, 82.50.Hp

$NiAl_2O_4$ Nanocomposite *via* Combustion Synthesis for Sustainable Environmental Remediation

Babu Nandana[1,3], Devadathan Dedhila[1,2], V. Baiju[1,2], and G. Sajeevkumar[1,2]

[1]*Nanoscience Research Laboratory, PG & Research Department of Physics, Sree Narayana College, Kollam, India*
[2]*University of Kerala, Senate House Campus, Palayam, Thiruvananthapuram-34, Kerala, India*
[3]*Department of Physics, Amrita School of Arts and Sciences, 690525 Amritapuri, Amrita Vishwa Vidyapeetham, India*

In the present study, $NiAl_2O_4$ nanocomposite was synthesized using solution combustion method. The sample was annealed at three different temperatures (500°C, 700°C and 900°C) to study the variations in properties attained with annealing temperature. Structural characterizations of all the synthesized samples were carried out using XRD, SEM, EDAX and FTIR analysis. From XRD, the formed metal oxides were confirmed to be $NiO/NiAl_2O_4$ nanocomposite. Crystallite sizes of these oxides were calculated using Scherrer equation. FTIR also confirmed the structure of metal oxides. All three samples showed strong UV-Vis absorption that made them suitable candidate for photocatalytic degradation of organic dyes. The photocatalytic degradation activity of all three synthesized nanocomposites on acidic dye (Congo red) were studied and compared. Results confirm that proper tuning of these nanocomposites could improve their photocatalytic activity.

У цьому дослідженні нанокомпозит $NiAl_2O_4$ був синтезований за допомогою методу спалювання розчину. Зразок відпалювали за трьох різних температур (500°C, 700°C і 900°C) для вивчення варіяцій властивостей, досягнутих за температури відпалу. Структурні характеризації всіх синтезованих зразків проводилися за допомогою рентґенівської дифракції, сканувальної електронної мікроскопії, енергорозсіювальної рентґеноспектральної електронно-зондової мікроаналізи й інфрачерво-

ної спектроскопії на основі перетвору Фур'є. З рентґенівської дифракції було підтверджено, що утворені оксиди металів є нанокомпозитом $NiO/NiAl_2O_4$. Розміри кристалітів цих оксидів були розраховані за Шеррerовою формулою. Аналіза інфрачервоної спектроскопії на основі перетвору Фур'є також підтвердила структуру оксидів металів. Всі три зразки показали сильне поглинання у видимій і ультрафіолетовій областях світла, що зробило їх придатними для фотокаталітичної деґрадації органічних барвників. Вивчено та порівняно фотокаталітичну деґрадаційну активність всіх трьох синтезованих нанокомпозитів на кислотному барвнику (конго червоному). Результати підтверджують, що правильна настройка цих нанокомпозитів уможливила б поліпшити їхню фотокаталітичну активність.

Key words: nanocomposites, solution combustion, nickel aluminate, photocatalytic activity, Congo red, acidic dye.

Ключові слова: нанокомпозити, горіння розчину, алюмінат ніклю, фотокаталітична активність, конго червоний, кислотний барвник.

(Received 15 May, 2021; in revised form, 19 May, 2021)

1. INTRODUCTION

Oxide spinels are an advanced group of materials in the solid-state sciences with great technological demand, being able to be applied as magnetic materials, semiconductors, pigments, catalysts, refractories, sensors, carriers and electronic ceramics [1–3]. They can be used as the carrier for catalysts due to their resistance to high temperatures, low surface acidity, and strong interaction with the noble metals, which provide chemical and physical stability [4].

Interest in the synthesis of partially inverted spinels-like nickel aluminates ($NiAl_2O_4$) nanoparticles has increased due to its different properties when compared to the corresponding bulk material such as excellent strength, high thermal stability, chemical inertia, good wettability with metals at high temperature, besides the general merits that the spinel materials have [1, 5]. Nickel aluminates ($NiAl_2O_4$) is a mixed cation oxide with normal spinel structure, where Al occupies the octahedral sites and Ni occupies the tetrahedral sites. Industrial application of this material is mainly based on its stable structure at high temperature and catalytic features. Prime importance of nickel aluminates for the catalytic applications ranging from methane/steam and methanol reforming to hydrocarbon cracking, dehydrogenation, hydrodesulphurization, and hydrodenitrogenation [6] are due to its high surface area that results from small particle size. In particular, the nickel aluminate can be used as a good ceramic skeleton for infiltration of metals at high temperature [7]. Industrial application of this material is mainly

based on its stable structure at high temperature and catalytic features. Hence, the synthesis of nanosize nickel-aluminate nanoparticles is worth studying [8–10].

Several preparation methods have been studied to obtain crystalline nickel aluminate spinels with small particle size, such as sol gel synthesis [11, 12], sonochemical method [10], microwave heating [13], polymer solution route [7] and solid-state reaction [14]. Recently solution combustion synthesis, an effective and versatile method are used by many researchers for the synthesis of different crystal structures. In the present work, $NiO/NiAl_2O_4$ nanocomposite was synthesized using the solution combustion-reaction method. In order to study the effects of annealing on the structural and optical properties of nickel aluminates, the synthesised materials were annealed at three different temperatures.

Recently, the removal of resultant hazardous organic pollutants in water sources from human productive activities has become an important research topic. Photocatalysis is a very promising low-cost advanced oxidation process based on the use of proper semiconductor materials, which upon activation with suitable light sources give rise to the formation of various reactive species. These reactive species react with organic contaminants that result in complete mineralization with no waste disposal problem. Important part of the present work was to study the application of $NiAl_2O_4$ nanocomposite as photocatalyst for the degradation of organic cationic dye—Congo red. The effect of annealing on the photocatalytic degradation of organic cationic dye was also studied and compared. The variations of dye concentration and catalyst dosage were also an objective of the present study.

2. EXPERIMENTAL DETAILS

A chemical reagent purchased from Merck was used. Nickel aluminates were prepared using solution combustion method. Aluminium-nitrate nonahydrate and nickel-nitrate dihydrate were used as starting materials. Ethylene glycol and urea were used as fuel and citric acid to control pH. 1 M aluminium-nitrate nonahydrate and nickel-nitrate dihydrate was taken in a beaker and 0.6 g of urea and 0.4 g of citric acid were added to it. 4 ml of ethylene glycol and 20 ml of distilled water are added to it drop by drop. The solution is stirred well until all the components are completely dissolved. The beaker is then placed in a combustion chamber. In the chamber, rapid heating of the solution took place, and once, the ignition point of fuel was reached the mixture burned to form the product. The powder obtained after combustion was annealed at 500°C, 700°C and 900°C for 4 hours in a muffle furnace to obtain the respective metal-oxide

nanoparticles. Samples were named as NAF, NAS and NAN for nickel aluminates annealed at 500°C, 700°C and 900°C, respectively.

Structural properties of the synthesised samples were studied using x-ray diffraction (XRD) and Fourier-transform infrared spectroscopy (FTIR). The powder x-ray diffraction patterns of the prepared samples were recorded using XPERT-PRO model powder diffractometer (PAN analytical, Netherlands) employing CuK_α radiation ($\lambda = 1.54060$ Å) operating at 40 kV, 30 mA by recording 2θ in the range of 10–70° at a scan rate of 0.5°/min. The FTIR spectrum of the produced samples were recorded using Perkin–Elmer FTIR Spectrophotometer in the wavenumber range 400 cm^{-1} and 4000

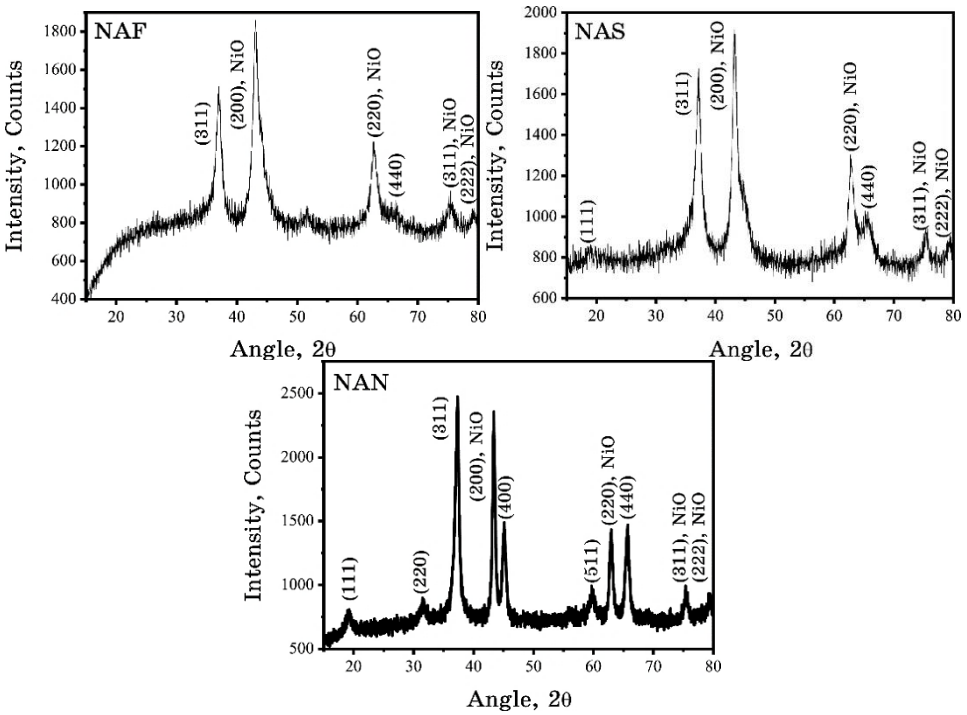

Fig. 1. XRD of NAF, NAS and NAN.

TABLE 1. Crystallite size of NAF, NAS and NAN estimated by means of using Scherrer equation.

Sample	Crystallite size, nm
NAF	7.93 ± 0.9
NAS	10.01 ± 1.52
NAN	13.87 ± 1.83

cm^{-1} by KBr disc method. Optical properties of the synthesized samples were studied using UV-visible (UV-Vis) absorption spectroscopy techniques. JASCO 650 UV-Vis spectrophotometer was used to record UV-Vis absorbance.

3. RESULTS AND DISCUSSIONS

3.1. XRD Analysis

X-ray diffractograms obtained for NAF, NAS and NAN are shown in Fig. 1. For confirming the structure of the prepared samples, 2θ values, relative intensities and interplanar spacing (d_{hkl}) values in the observed diffraction peaks were compared with the standard values as reported by JCPDS-ICDD Centre for Diffraction Data. Data were compared with pattern number #10-0339 of $NiAl_2O_4$. In addition to peaks of $NiAl_2O_4$, additional peaks were observed. Hence, the data were also compared with pattern number #46-1215 of Al_2O_3 and pattern number #78-0429 of NiO. From the results, it was seen that both NiO and $NiAl_2O_4$ were present in the prepared samples with complete absence of Al_2O_3. NAF and NAS showed predominance of NiO, whereas NAN showed the dominance of $NiAl_2O_4$ peaks. According to JCPDS-ICDD pattern number #10-0339, $NiAl_2O_4$ is a cubic system with f.c.c. lattice, and JCPDS-ICDD pattern number #78-0429 showed NiO as a cubic system with f.c.c. lattice. Hence, the system formed will be a cubic system with f.c.c. lattice.

The average crystallite or grain size was calculated using the Scherrer equation as follows:

$$D = \frac{K\lambda}{\beta \cos\theta}, \tag{1}$$

where θ and λ are the Bragg angle and the wavelength of the x-ray used, respectively. K is a constant approximately equal to 0.9; β is the full width at half-maximum corresponding to the intense peak at θ value. Table 1 gives the crystallite sizes of synthesized samples. It is found that the crystallite size and crystallinity of the synthesized samples increased with increase in annealing temperature. The XRD results confirm the formation of heterostructure of $NiO/NiAl_2O_4$ nanocomposite.

3.2. SEM Analysis

The SEM image of NAN at 1 μ magnification is shown in Fig. 2. NAN shows Coral reef with high level of porosity.

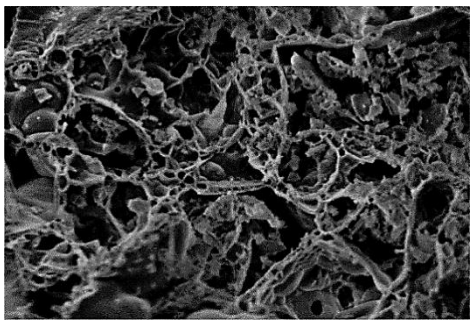

Fig. 2. SEM analysis of nickel-aluminate sample annealed at 900°C.

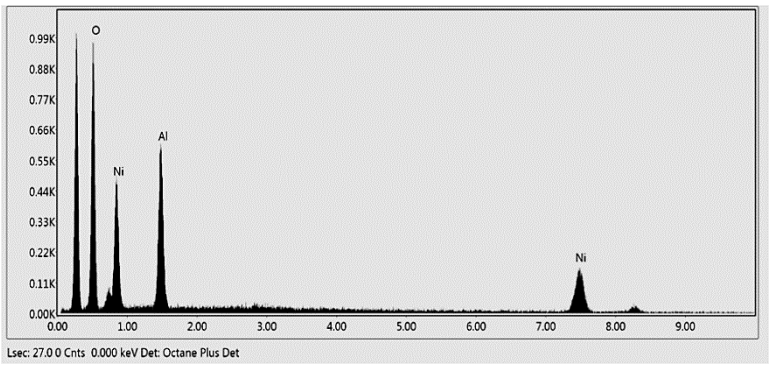

Fig. 3. EDAX analysis of nickel-aluminate sample annealed at 900°C.

3.3 EDAX Analysis

Figure 3 shows the EDAX spectrum of NAN. The absence of impurity peaks confirms the purity of synthesized metal-oxide samples. It is found to have 19.97% of aluminium, 25.37% of nickel and 54.66% of oxygen.

The FTIR spectrum of the $NiO/NiAl_2O_4$ heterostructure at different temperatures is shown in Fig. 4. The OH-bending modes of NAF, NAS and NAN were observed at 1372, 1375 and 1373 cm^{-1}, respectively. Metal oxides give absorption bands below 1000cm^{-1} arising from interatomic vibrations. For NAF, NAS and NAN, the peaks obtained near 412, 410 and 409 cm^{-1} give evidence about the presence of NiO [15]. The peak corresponding to Al–O bond in the range 727–704 cm^{-1} is found to show a noticeable intensity gain with rise in temperature. Hence, the FTIR studies agree with the XRD results. The bands above 1500 cm^{-1} could be assigned to the O–C=O symmetric and asymmetric stretching vibrations, which could be attributed to physical adsorption of CO_2 in air, when FTIR

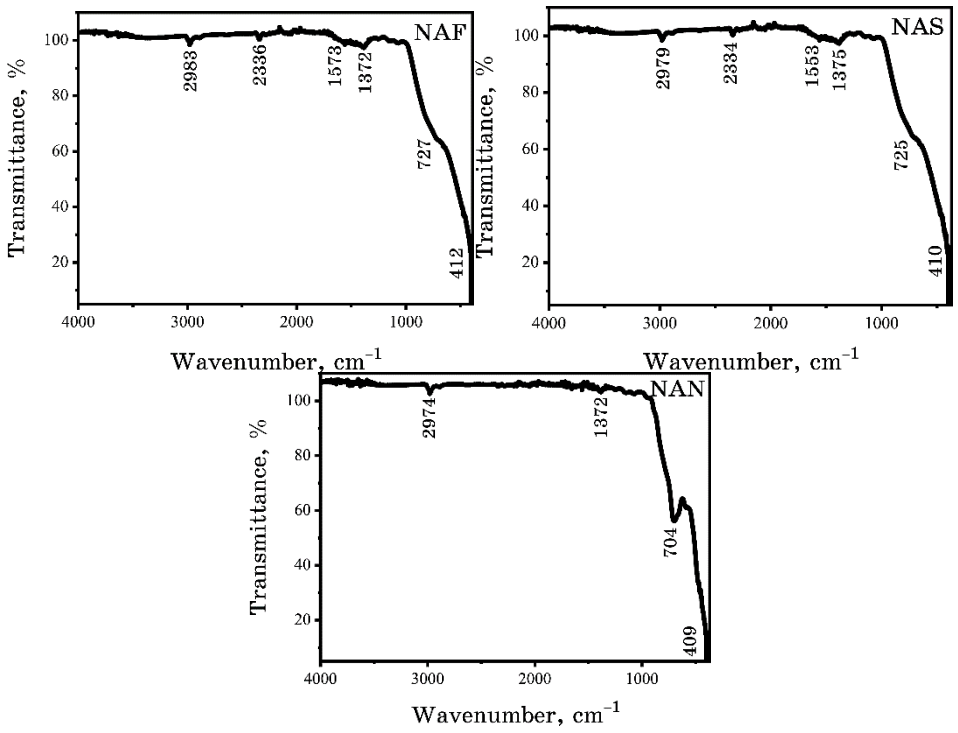

Fig. 4. FTIR spectra of NAF, NAS and NAN.

sample disks were prepared in an open air [16].

3.5 UV-Vis Absorbance Analysis

The UV/Vis absorption spectra of the NAF, NAS and NAN are shown in Fig. 5. All three samples showed three small bands around 380 nm, 575 nm and 650 nm that was similar to observations done by Ragupathi *et al.*, and these bands correspond to the formation of $NiO/NiAl_2O_4$ inverse spinel structure that is occurred [8]. The absorbance spectral analysis confirms the complete formation of a $NiAl_2O_4$ spinel structure [6] in the composite. The absorption bands located around 250 nm originate from the fundamental band-to-band electron transition. The variation in absorbance peaks of NAF, NAS and NAN could be attributed to the increasing predominance of nickel aluminate with annealing temperature.

From absorbance spectrum, Tauc plot was drawn, and the corresponding energy gap was found. The energy band gap of the material is related to the absorption coefficient α by the Tauc relation, $\alpha = A(h\nu - E_g)^n$, where A is a constant, $h\nu$ is the photon energy

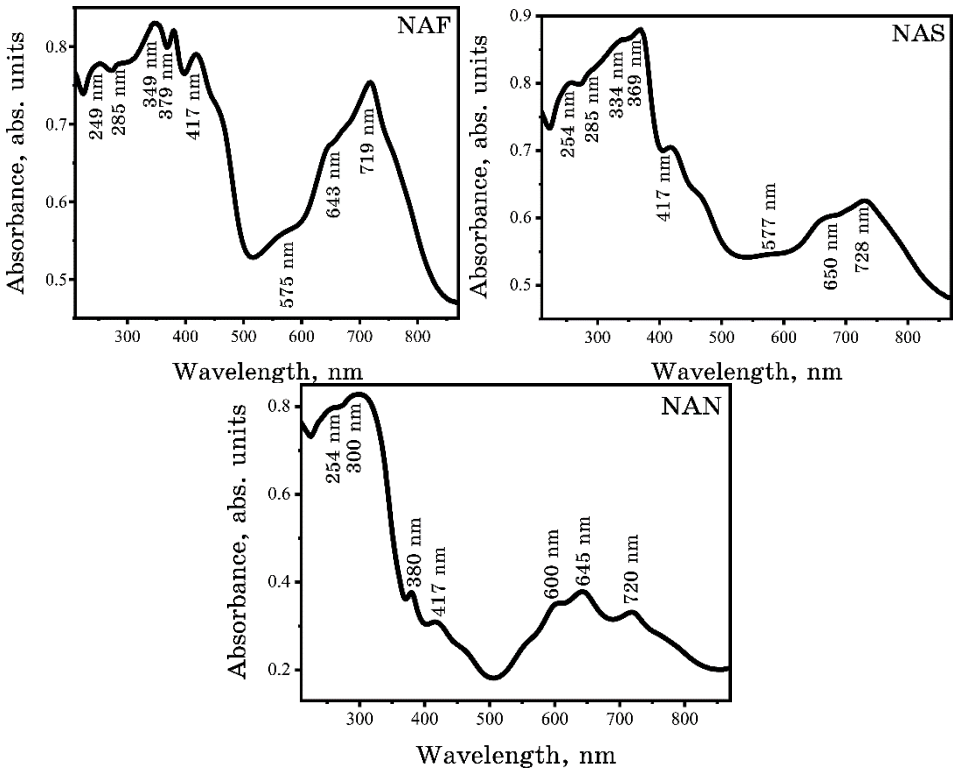

Fig. 5. UV-Vis absorbance spectra of NAF, NAS and NAN.

($\nu = c/\lambda$), E_g is the band gap, and n is either 2 for an indirect transition or ½ for a direct transition. The $(\alpha h\nu)^2$ *vs.* $h\nu$ for all the samples was also plotted. Figure 6 shows Tauc plots drawn. Table 2 shows the energy-band gaps obtained. The changing band gaps could also be attributed to the changing predominance of nickel aluminate with annealing temperature. The presence of additional bands is due to the presence of defects levels.

4. PHOTOCATALYTIC DEGRADATION STUDIES

The main objective of the present work is to study the application of nickel aluminates as photocatalyst for the degradation of organic cationic dye—Congo red. The various factors affecting photocatalytic-degradation-like effect of contact time, amount of photocatalyst and dye concentration were also investigated. Under UV illumination in a homemade photoreactor equipped with three 18W UV lamps with a wavelength of 254 nm, the photocatalytic-degradation studies were done. The UV-Vis absorbance spectrum of pure Congo

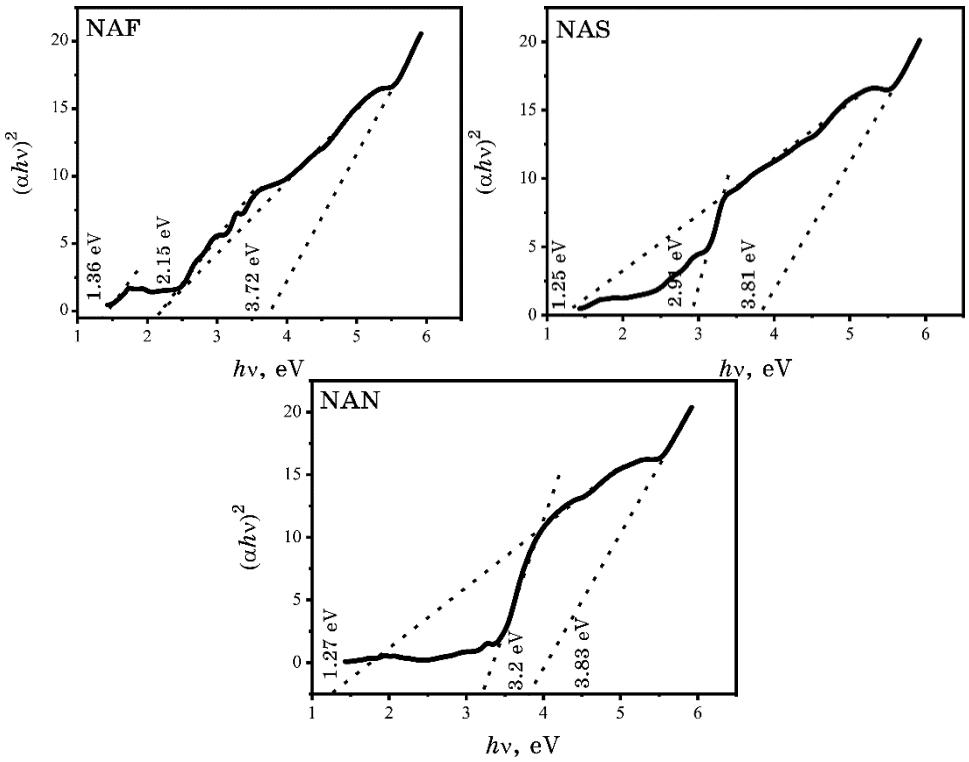

Fig. 6. Tauc plot of NAF, NAS and NAN.

TABLE 2. Energy-band gap obtained for NAF, NAS and NAN.

Samples	NAF	NAS	NAN
Energy band gap, eV	1.36	1.25	1.27
	2.15	2.91	3.2
	3.72	3.81	3.83

red (CR) absorbs at λ_{max} values of 344 nm and 498 nm, and for photodegradation studies, the λ_{max} value of 498 nm was taken as reference for CR. Figure 7 shows the absorbance spectrum of CR for 50-ppm concentration.

To study the effect of contact time on the photodegradation, Congo red dye solution with concentration of 300 ml of 50 ppm CR with 0.1 g of the photocatalyst kept at 300 K was kept under UV light. After desired time intervals (30, 60, 90 and 120 min), 10 ml of the solution was taken out and centrifuged, and UV-Vis absorption spectra were recorded. The amount of photocatalyst was varied from 0.025 g to 0.15 g to study its effect on photodegradation. Dye

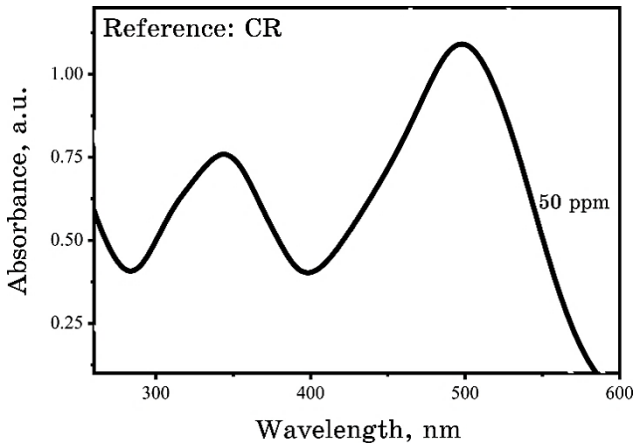

Fig. 7. The absorbance spectrum of CR for 50-ppm concentration.

solutions of three different concentrations were selected (25 ppm, 50 ppm and 75 ppm) to study the effect of initial dye concentration on photodegradation efficiency.

The photocatalytic degradation efficiency was calculated as follows:

$$\text{Photocatalytic Degradation Efficiency [\%]} = \frac{C_0 - C_t}{C_0} \times 100, \quad (2)$$

where C_0 is initial concentration of dye solution [mg·L^{-1}], C_t—final concentration of dye solution [mg·L^{-1}].

The photodegradation efficiency of 50 ppm CR dye solution, using NAF after 120 minutes, was found to be of 54.62%, whereas for NAS, it was found to be of 56.68%, and for NAN, it was of 88.91%. The absorption plots corresponding to the photodegradation of CR at different time intervals are shown in Fig. 8, and it is evident that the absorption peak shows a decrease in peak intensity with increase in time. The results show high rate of photodegradation of the dye with increase in contact time. The contact time in the experiment was fixed at 120 min. However, after 180 min, complete degradation of CR was observed for NAN photocatalyst. Here, the heterostructure with maximum predominance in nickel aluminate NAN showed maximum activity. This could be due the improved photocatalytic activity of nickel aluminate over nickel oxide and surface properties attained due to composite formation.

The amount of catalyst loading is one of the key parameters for the degradation efficiency. The results showed that, when catalyst dosage was increased up to 0.075 g, the percentage decolourization increased. The increase in dosage of the catalyst beyond 0.1 g re-

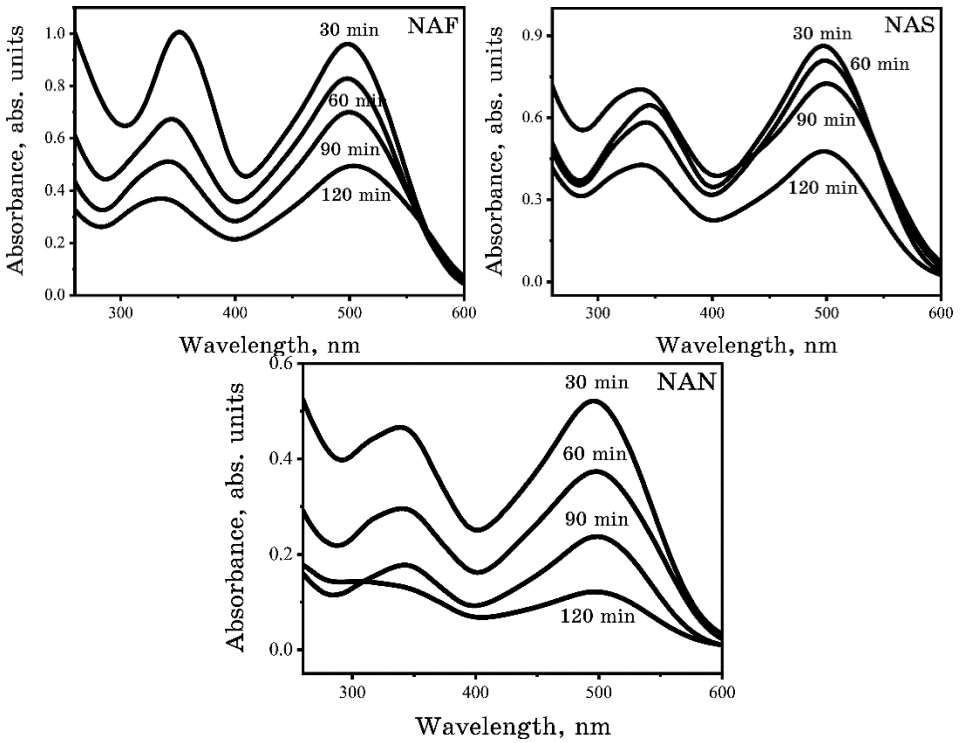

Fig. 8. Photocatalytic degradation of Congo red with using NAF, NAS and NAN.

sulted in a slight decrease in the degradation percentage. The increase in the catalyst loading increased the degradation rate that is due to the increase in total active surface area [17]. The increase in photocatalyst generates higher amount of hydroxyl radical through the interaction of UV light with photocatalyst. However, above 0.1 g, the percentage degradation significantly decreased due to decrease of formation of hydroxyl radicals. The catalyst loading affects both the number of active sites on photocatalysts and the penetration of UV light through the suspension [18]. With increasing catalyst loading, the number of active sites increases, but the penetration of UV light decreases due to shielding effect [19].

The effect of initial dye concentration on the rate of photocatalytic degradation for synthesized composites was studied, and the results obtained. The results indicate that the rate of photocatalytic degradation decreased with the increasing initial dye concentration. Increase in initial concentration of a dye increases the colour of dye solution that results in less penetration of light to the surface of the catalyst, and the number of excited dye molecules is decreased

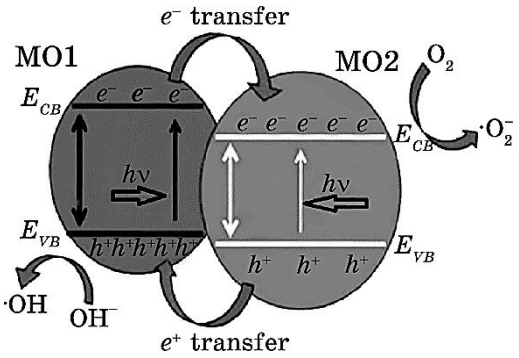

Fig. 9. Schematic representation of the photocatalytic degradation process.

[20].

When coupled heterostructure metal-oxide nanocomposite is irradiated by light, the electrons in the valence band (*VB*) of $NiAl_2O_4$ and NiO are excited to their conduction bands (*CB*) or to the defect levels presented in the band gap. The excited electrons from higher level *CB* of a metal oxide are transferred to the low-lying *CB* of the other member. Similarly, the holes are transferred from the low-lying *VB* to the *VB* band of the other metal oxide. This, in turn, leads to the efficient separation of photogenerated electron–hole pairs, increasing the recombination time of electrons and holes generated, and enhances the photocatalytic activity of the $NiO/NiAl_2O_4$. Figure 9 shows the schematic representation of the activity of the photocatalyst formed in the present work. Here, MO1 and MO2 represent the two metal oxides whose heterostructure is formed. In the absence of photocatalyst, it was found that CR dye is difficult to be oxidized by using UV light alone. Compared to a single semiconductor metal oxide, composites always increase photocatalytic activity, as they are very effective in separating photogenerated electron–hole pairs and increasing their recombination time.

5. CONCLUSION

In the present work, heterostructure of $NiO/NiAl_2O_4$ nanocomposite was synthesized using solution combustion method. The samples were annealed at 500°C, 700°C and 900°C to study the variations in properties attained with annealing temperature. Structural characterizations of all the synthesized samples were carried out using XRD, SEM, EDAX and FTIR analysis, which confirmed the formation of $NiO/NiAl_2O_4$ nanocomposite. XRD also showed that, as annealing temperature increased, the predominance of $NiAl_2O_4$ was increased. Crystallite sizes of these oxides were calculated using

Scherrer equation. All three samples showed strong UV-Vis absorption. UV-Vis absorption supported the transformation seen in XRD studies. The photocatalytic activity of all the synthesized nanoparticles was studied and compared, using Congo red. Activity was found to be high in case of NAN-kind $NiO/NiAl_2O_4$ nanocomposite sample annealed at 900°C. Proper tuning of the nanoparticles is expected to improve its photocatalytic activity.

REFERENCES

1. C. K. Stella and S. A. Nesaraj, *Iranian J. of Mat. Sci. & Eng.*, **7**, No. 2: 36 (2010).
2. L. Gama, M. A. Ribeiro, B. S. Barros, R. H. A. Kiminami, I. T. Weber, and A. C. F. M. Costa, *Journal of Alloys and Compounds*, **483**, Nos. 1–2: 453 (2009); https://doi.org/10.1016/j.jallcom.2008.08.111
3. N. M. Deraz, *International Journal of Electrochemical Science*, **8**: 5203 (2013).
4. F. P. R. Nielson, C. R. N. Raimundo, F. M. Silvia, M. V. M. S. Mariana, and S. Martin, *International Journal of Hydrogen Energy*, **35**, No. 21: 11725 (2010); https://doi.org/10.1016/j.ijhydene.2010.08.024
5. A. R. Phani, M. Passacantando, and S. Santucci, *Mater. Chem. Phys.*, **68**, Nos. 1–3: 66 (2001); https://doi.org/10.1016/S0254-0584(00)00270-4
6. C. Ragupathi, J. J. Vijaya, and L. J. Kennedy, *J. Saudi Chem. Soc.*, **21**: S231 (2017); https://doi.org/10.1016/j.jscs.2014.01.006
7. J. W. Kim, P. W. Shin, M. J. Lee, and S. J. Lee, *J. Ceramic Processing and Research*, **7**: 117 (2006).
8. C. Ragupathi C, J. J. Vijaya, P. Surendhar, and L. J. Kennedy, *Polyhedron*, **72**: 1 (2014); https://doi.org/10.1016/j.poly.2014.01.013
9. J. P. Kumar, G. K. Prasad, J. A. Allen, P. V. R. K. Ramacharyulu, K. Kadirvelu, and B. Singh, *Journal of Alloys and Compounds*, **662**: 44 (2016); https://doi.org/10.1016/j.jallcom.2015.11.181
10. P. Jeevanandam, Y. Koltypin, and A. Gedanken, *Materials Science and Engineering: B*, **90**, Nos. 1–2: 125 (2002); https://doi.org/10.1016/S0921-5107(01)00928-X
11. C. O. Arean, M. P. Mentruit, A. J. L. Lopez, and J. B. Parra, *Colloids and Surfaces A: Physicochemical and Engineering Aspects*, **180**, No. 3: 253 (2001); https://doi.org/10.1016/S0927-7757(00)00590-2
12. F. Meyer, R. Hempelmann, S. Mathur, and M. Veith, *J. Mater. Chem.*, **9**, No. 8: 1755 (1999); https://doi.org/10.1039/A900014C
13. M. M. Amini and L. Torkian, *Matterials Lett.*, **57**, No. 3: 639 (2002); https://doi.org/10.1016/S0167-577X(02)00845-5
14. A. Yamakawa, M. Hashiba, and Y. Nurishi, *J. Mater. Sci.*, **24**, No. 4: 1491 (1989); https://doi:10.1007/bf02397091
15. M. A. Gondal, A. S. Tawfik, and Q. A. Drmosh, *Applied Surface Science*, **258**, No. 18: 6982 (2012); https://doi.org/10.1016/j.apsusc.2012.03.147
16. S. V. Ganachari, R. Bhat, R. Deshpandeand, and A. Venkataraman, *Recent Research in Science and Technology*, **4**: 50 (2012).
17. M. S. T. Goncalves, A. M. F. Oliveira-Campose, E. M. M. S. Pinto,

P. M. S. Plasencia, and M. J. R. P. Queiroz, *Chemosphere*, **39**, No. 5: 781 (1999); https://doi.org/10.1016/S0045-6535(99)00013-2

18. N. Daneshvar, D. Salari, and A. R. Khataee, *J. Photochem, Photobiol. A: Chem.*, **157**, Iss. 1: 111 (2003); https://doi.org/10.1016/S1010-6030(03)00015-7
19. C. A. K. Gouvea, F. Wypych, S. G. Moraes, N. Durán, N. Nagata, and P. P. Zamora, *Chemosphere*, **40**, No. 4: 433 (2000); https://doi.org/10.1016/S0045-6535(99)00313-6
20. N. Daneshvar, N. D. Salari, and A. R. Khataee, *J. Photochem. Photobiol. A: Chem.*, **162**, Issues 2–3: 317 (2004); https://doi.org/10.1016/S1010-6030(03)00378-2